

## *Ab initio* study of larger $Pb_n$ clusters stabilized by $Pb_7$ units possessing significant covalent bonding

Haisheng Li,<sup>1</sup> Yong Ji,<sup>1</sup> Fei Wang,<sup>1,2</sup> S. F. Li,<sup>1,2</sup> Q. Sun,<sup>1,2</sup> and Yu Jia<sup>1,2,\*</sup><sup>1</sup>Laboratory of Condensed Matter Theory and Computational Materials, Zhengzhou University, Zhengzhou 450052, People's Republic of China<sup>2</sup>Laboratory of Clean Energy and Quantum Structures, and School of Physics and Engineering, Zhengzhou University, Zhengzhou 450052, People's Republic of China

(Received 4 October 2010; revised manuscript received 21 December 2010; published 24 February 2011)

First-principles calculations within the density-functional theory (DFT) have been carried out to study the geometric and electronic structures of  $Pb_n$  clusters with dimensions of up to 3 nm. As distinguished from prolate silicon, germanium, and tin clusters, amorphouslike lead clusters containing more independent pentagonal bipyramid  $Pb_7$  units are more favorable than octahedral ( $O_h$ ) fragments as  $n$  up to 147. On the other hand, covalently bonded  $Pb_7$  units obstruct the electronic delocalization process, i.e., the transition from clusters to metallic bulk characters. The average bond length (charge density) within the  $Pb_7$  unit is usually shorter (higher) than that among the  $Pb_7$  units. By tracing two kinds of bond forms in the  $Pb_7$  unit and between  $Pb_7$  units, we find that the melting process begins from the weaker bond between the  $Pb_7$  units. The existence of significant covalent bonding in metal clusters may also generally hold for explaining why some Sn and Pb clusters also remain solid above the bulk melting temperature as previously reported.

DOI: 10.1103/PhysRevB.83.075429

PACS number(s): 61.46.Bc, 73.22.-f, 31.15.A-, 36.40.-c

### I. INTRODUCTION

Owing to the large surface-volume ratio and novel electronic structures, clusters usually show a lower melting temperature, a higher magnetic moment, and better catalysis than their bulk counterparts. These intriguing physical and chemical properties render cluster processes.<sup>1-3</sup> From insulator to semiconductor and metal, group-IV elements are very special in the Periodic Table, and therefore, their clusters are also expected to exhibit unique properties, especially for their binding forms, growth patterns, and nonmetal-metal transitions. Previous studies revealed that the growth modes of silicon,<sup>4-10</sup> germanium,<sup>11-15</sup> and tin<sup>16-22</sup> clusters adopt prolate structures when cluster sizes are lower than 27, 40, and 35, respectively, owing to covalent bonding. However, for lead clusters, near-spherical structures have been predicted for all sizes.<sup>23</sup> On the other hand, both the stabilities and the electronic properties of Pb films on substrates are strongly dependent on the film thickness, owing to the strong quantum size effect.<sup>24-27</sup> For the above reasons, the divergence between Pb clusters and the other group-IV elements together with the growth process from Pb clusters to its bulk is worth studying.

Experimentally, a photoionization mass spectroscopy analysis showed that  $Pb_7$ ,  $Pb_{10}$ ,  $Pb_{13}$ , and  $Pb_{17}$  are magic clusters, while  $Pb_{14}$  and  $Pb_{18}$  are hard to be observed.<sup>28-30</sup> Photoelectron spectroscopy and theoretical evidence also manifested that  $Pb_{12}^{2-}$  is a highly stable icosahedral ( $I_h$ ) cage cluster and bonded by four delocalized radial  $\pi$  bonds and nine delocalized on-sphere  $\sigma$  bonds from the  $6p$  orbitals of the Pb atoms.<sup>31</sup> Lüder *et al.*<sup>32</sup> also carried out photoelectron spectroscopy experiments to measure vertical detachment energies (VDEs) of  $Pb_n$  anions, showing that pronounced peaks are visible at  $Pb_7$  and  $Pb_{10}$ . Peredkov *et al.*<sup>33</sup> suggested a method for determining the cluster size and determined core-level binding energies for free large lead clusters with values that approach infinite bulk. With strong deviation from the metallic droplet and jellium models, core-level photoelectron spectroscopy

experiments showed reduced electronic shielding once the cluster size falls below  $\sim 20$  atoms.<sup>34</sup>

Theoretically, many studies have also been carried out on both the geometrical structures and electronic properties of Pb clusters. Wang *et al.*<sup>35</sup> studied the geometric and electronic structures of  $Pb_n$  ( $n = 2-22$ ) clusters by using the Becke-Lee-Yang-Parr (BLYP) functional calculation combined with an empirical genetic algorithm simulation, and concluded that the  $Pb_{13}$ ,  $Pb_{15}$ ,  $Pb_{17}$ , and  $Pb_{19}$  are less stable than their neighbors.<sup>23,29</sup> Rajesh *et al.*<sup>36,37</sup> studied the geometrical structures of neutral and charged  $Pb_n$  ( $n = 2-15$ ) clusters based on *ab initio* molecular-dynamics (MD) simulations and concluded that  $Pb_4$ ,  $Pb_7$ ,  $Pb_{10}$ ,  $Pb_{13}$ , and their corresponding cations are magic clusters with compact structures, in accordance with the experiments mentioned above.<sup>28-30</sup> Li *et al.*<sup>38</sup> performed global structural optimizations for neutral lead clusters  $Pb_n$  ( $n = 2-20$ ) by using a genetic algorithm (GA) coupled with a tight-binding (TB) potential, and found that  $Pb_n$  ( $n = 4, 7, 10, 13, 15$ , and  $17$ ) clusters are stable. Using a many-body glue potential for lead, Hendy *et al.*<sup>39</sup> identified two icosahedral series which have the lowest energies of any known structure in the size range from 900 to 15 000 Pb atoms. However, few further studies showed the growth mode of medium-sized Pb clusters systematically. Interestingly, Pushpa *et al.*<sup>40</sup> recently suggested the melting point of small Pb clusters is higher than Pb bulk, in contrast to the common belief that clusters are more active than their bulk counterparts owing to surface effects, and Luo *et al.*<sup>41</sup> showed that the surface free-energy difference between solid and liquid phase is a decisive factor for the size-dependent melting of nanomaterials.

However, the underlying essential physical mechanism of the above intriguing phenomena<sup>40,41</sup> in Pb clusters is still open, and some key questions should be further elucidated: (1) What are the geometric structures and the growth modes of the medium-sized  $Pb_n$  clusters; (2) what is the characteristic bonding mode in these clusters? To answer the above questions, we performed the density-functional theory (DFT)

calculations on both the geometric and electronic properties of  $Pb_n$  clusters up to a very large size. We find that the  $Pb_7$  cluster can be regarded as a fundamental unit in larger clusters, and  $Pb_7$  unit-based clusters are more energetically favorable than  $O_h$  fragments as the cluster size is up to 80 atoms. For larger cluster  $Pb_{147}$  ( $Pb_{309}$ ), the  $I_h$  structure is more (less) stable than its corresponding  $O_h$  isomer. The analyses of electronic density of states and charge density difference, together with other properties, show that the covalent bonding in the  $Pb_7$  units not only enhances the stabilities of larger clusters, but also reduces the electronic delocalization and suspends the transition from clusters to metallic bulk characters. Correspondingly, these findings may support the bond stiffening theoretical prediction that  $Pb_n$  nanoclusters possess a higher melting point than that of their bulk counterparts,<sup>40</sup> and the underlying physical picture of the existence of significant covalent bonding in metal clusters may also hold for explaining why some Sn and Pb clusters also remain solid above the bulk melting temperature.<sup>42–44</sup>

## II. DETAILS OF CALCULATION METHODS

Our calculations are based on the DFT with the spin-polarized generalized gradient approximation (GGA)<sup>45</sup> implemented in the VASP code.<sup>46,47</sup> The interactions between the valence electrons and the ionic cores are described by the projector augmented wave (PW91) method.<sup>48,49</sup> The wave function is expanded in a plane-wave basis with an energy cutoff of 98 eV. The geometric structures are optimized by the conjugated gradient (CG) method.<sup>50</sup> We choose a simple cubic supercell with a side size of 25 Å in periodic boundary conditions to simulate an isolated  $Pb_n$  cluster for  $n$  ranging from 2 to 80. The larger simple cubic unit cells are used for larger cluster calculations to make sure that there is at least 10 Å between clusters in the neighboring cells. The Brillouin zone is only represented by the gamma point, the total energy is converged up to  $10^{-4}$  eV for the electronic structure relaxations, and the convergence criterion for the force on each ion is taken to be 0.02 eV/Å. The spin polarization calculation is also considered for cluster sizes of less than 40 atoms. The calculated bond length of the  $Pb_2$  dimer and the lattice constant of Pb bulk are 2.93 and 5.03 Å, respectively, which are in good agreement with the calculated values of 2.91 and 5.05 Å,<sup>36,51</sup> respectively.

To search for the most stable cluster structures, three different methods are adopted to obtain the initial input structures in our calculations. First, we take many available configurations as the initial input structures, as reported in previous literatures,<sup>4–22</sup> including some highly symmetric configurations, such as  $I_h$  and  $O_h$ -based fragments, and low symmetries as well. In this line, we obtained some stable low-lying structures. Second,  $Pb_{n-m}$  ( $Pb_{n+m}$ ) can be obtained by randomly removing (adding)  $m$  atoms from (on) the low-lying isomers of the  $Pb_n$  cluster obtained in the first step, which provides a rapid way to obtain as many initial structures as possible. Finally, to break the limitations of the above two methods, we carry out the *ab initio* MD simulations on some low-lying isomers to produce random structure seeds, which was verified as a powerful method to determine the ground states of nanoclusters in our previous work.<sup>52</sup> In our MD simulations, the time of each step is taken to be 1 fs and the

total simulation time lasts 5 ps, with the temperature ranging from 1000 to 0 K, including constant temperature annealing.

## III. THE STABILITY OF $Pb_n$ CLUSTERS: $Pb_7$ AS A FUNDAMENTAL UNIT IN LARGER CLUSTERS

To elaborate on the stabilities of  $Pb_n$  clusters, we give the average binding energy of a given cluster,

$$E_b = -[E(Pb_n) - nE(Pb_{\text{atom}})]/n. \quad (1)$$

$E(Pb_{\text{atom}})$  and  $E(Pb_n)$  are the total energies of a single Pb atom and  $Pb_n$  cluster from our DFT calculations, respectively. As a test, the properties of ground-state  $Pb_n$  ( $n=2–15$ ) are in good agreement with those reported in Ref. 36, except that  $Pb_n$  ( $n=2, 3, 5$ ) has a  $2\mu_B$  magnetic moment, and the other  $Pb_n$  clusters studied in this paper are uniformly nonmagnetic. From  $Pb_7$  to  $Pb_{13}$ , the stable clusters prefer to form a complete  $I_h$  structure as soon as possible, except for  $Pb_{10}$ . In detail, the stable  $Pb_7$  ( $D_{5h}$ ) is a pentagonal bipyramid with a binding energy of 2.62 eV/atom. For  $Pb_8$  and  $Pb_9$  ( $C_{2v}$ ), an edge-atom-capped bipyramid ( $Pb_7$ ) and the coupling of two  $Pb_7$  (with five common atoms) are favored, respectively. The  $Pb_{10}$  cluster prefers a capped trigonal prism. The  $Pb_{11}$  ( $C_{2v}$ ) can be obtained by adding four atoms on the neighboring facets of the  $Pb_7$ , the  $Pb_{12}$  is a distorted  $I_h$  hollow cage, and the  $Pb_{13}$  favors a perfect  $I_h$  structure. The stable  $Pb_{14}$  is an edge-capped  $Pb_{13}$  and the  $Pb_{15}$  is an encapsulated hexagonal antiprism. Although the binding energy of our results is larger than that in Ref. 36, the oscillation trend and the second-order difference of energies, together with the configurations of low-lying isomers of  $Pb_n$  ( $n=2–15$ ), are in good agreement with those of Rajesh *et al.*<sup>36,37</sup> and the experimental results.<sup>23,29</sup>

One intriguing discovery is that  $Pb_n$  clusters usually contain more independent pentagonal bipyramid  $Pb_7$ . The structures and binding energies of the most stable  $Pb_n$  ( $n=16–37$ ) isomers are presented in Fig. 1. For convenience, we classify the atoms in Pb clusters as surface and inner atoms. To guide the eyes, the inner atoms belonging (not belonging) to  $Pb_7$  units are pictured in red (yellow), while inner atoms in  $O_h$  fragments are also in red in Fig. 2. From Fig. 1, one can find that larger  $Pb_n$  clusters consist of significant  $Pb_7$  units, with the inner atom (in red) acting as the cap atom of the pentagonal bipyramid structure. For example, as indicated in Fig. 1, from  $Pb_{20}$  to  $Pb_{25}$ ,  $Pb_n$  contains two isolated  $Pb_7$  units, which are coupled with six (for  $Pb_{20}$ ) to 11 (for  $Pb_{25}$ ) glue atoms, while smaller Pb clusters ( $n=16–19$ ) can be viewed as consisting either of one intact  $Pb_7$  unit or more  $Pb_7$  blocks sharing the same capping atom. For larger  $Pb_n$  clusters,  $n=28–32$  and  $n=33–37$ , three and four isolated integral  $Pb_7$  units are identified, respectively. We also note that from  $Pb_{19}$  to  $Pb_{20}$ , the structure transforming from a one-atom-centered configuration to a two-atom-centered structure is also supported by a core-level photoelectron spectroscopy experiment, which showed reduced electronic shielding once the cluster size falls below  $\sim 20$  atoms.<sup>34</sup> Coincidentally, our results are in good agreement with the work published recently.<sup>53</sup> Note also that the prolate growth modes of  $Si_n$ ,  $Ge_n$ , and  $Sn_n$  (Refs. 4–22) are unfavorable for  $Pb_n$  ( $12 < n < 45$ ) clusters.

To check the stabilities of the  $Pb_7$  unit-based growth mode mentioned above, we further carried out studies on larger  $Pb_n$

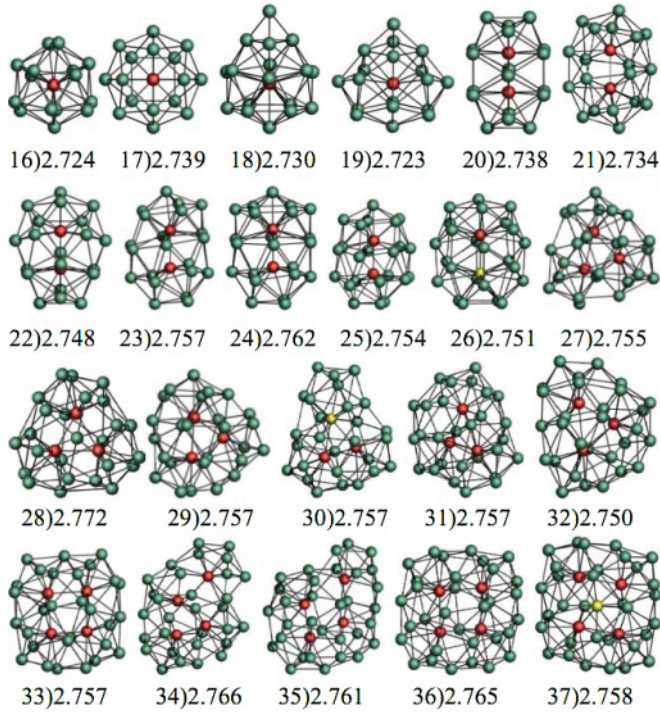


FIG. 1. (Color online) The structures and binding energies of the ground state of Pb<sub>n</sub> ( $n = 16-37$ ) isomers. The average binding energies  $E_b$  (eV/atom) with respect to the isolated Pb atom defined by  $E_b = -[E(\text{Pb}_n) - nE(\text{Pb}_{\text{atom}})]/n$ . Inner atoms forming (not forming) Pb<sub>7</sub> units are pictured in red (yellow), respectively.

clusters up to  $n = 85$ . In Fig. 2(a), the binding energies of Pb<sub>7</sub> unit-based clusters (line with hexagons) are higher than  $O_h$  fragments (line with triangle) up to  $n = 85$ . Under the triangle symbols are the structures of  $O_h$  fragments. For convenience, we describe the Pb<sub>7</sub> unit-based clusters and the  $O_h$  fragments of a given Pb<sub>n</sub> cluster as  $Na$  and  $Nb$ , respectively. 38a has five Pb<sub>7</sub> units and the binding energy is 2.76 eV/atom, which is more stable by 0.03 eV/atom than the truncated  $O_h$  38b (with six center atoms). 41a can form four Pb<sub>7</sub> units and the surface atoms connect each other with triangles, making it a magic cluster. Owing to the coupling of five stable Pb<sub>7</sub> units, the cluster 44a lies higher in the binding energy than that of the six-atom-centered 44b ( $O_h$ ) by 0.03 eV/atom. The four stable Pb<sub>7</sub> unit-coupled structure 52a is (0.01 eV/atom) more stable than the ten-atom-centered structure 52b. As the cluster size increases, this trend can be clearly seen in Fig. 2(a). Once again, we show that the Pb<sub>7</sub> unit can be regarded as a block in larger clusters. Interestingly, if we take the  $I_h$  symmetry as an initial structure, the Pb<sub>55</sub> will relax to a low-symmetry configuration, which has four independent Pb<sub>7</sub> units. This is an unexpected result as it is well known that a closely packed  $I_h$  structure is usually regarded as the ground-state structure of many metal clusters. In fact, the most stable structure of Pb<sub>55</sub> [in Fig. 2(a)] can contain six independent Pb<sub>7</sub> units, which is the coupling of two magic clusters Pb<sub>28</sub> (in Fig. 1). Exactly speaking, we cannot guarantee that the obtained most stable structures are absolutely the ground-state configurations, and some of them may be merely some low-lying isomers in the whole potential space, especially for  $n > 20$  in the current computational levels. However, our results can solidly

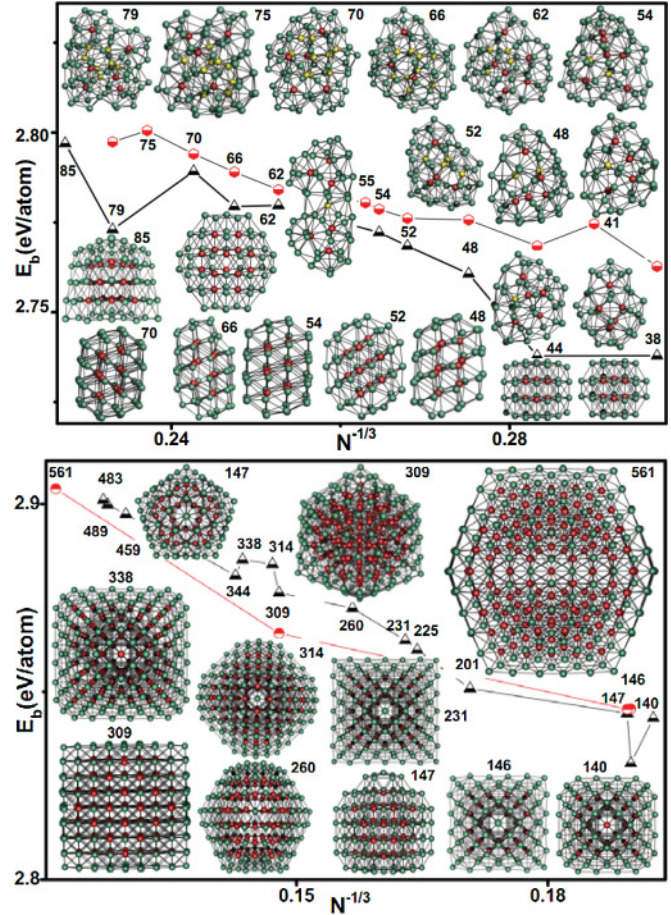


FIG. 2. (Color online) The structures and binding energy as a function of  $n^{-1/3}$ . Inner atoms forming (not forming) Pb<sub>7</sub> units are pictured in red (yellow), while inner atoms of  $O_h$  fragments are also in red. The red hexagons (circles) and black triangles correspond to the Pb<sub>7</sub> based clusters and  $O_h$  fragments, respectively.

support that larger Pb<sub>n</sub> clusters favor morphology structures composing Pb<sub>7</sub> units.

As well known, bulk Pb possesses a closely packed fcc structure, so it is meaningful to study the critical size at which the phase transition from Pb<sub>7</sub> unit-based structures to fcc occurs. With the most compact atom arrangement in plane and the largest spacing between planes, the (111) surface of fcc metals is usually favorable for crystal and cluster growth. Using variable-temperature scanning tunneling microscopy, Thürmer *et al.*<sup>54</sup> grew the micrometer-sized Pb(111) crystallites on the top of the Ru(0001). A flattop Pb(111) single-crystal island grown on Si(111)-(7×7) was also observed by a scanning tunneling microscopy (STM) image.<sup>55</sup> Recently, Kumar *et al.*<sup>2</sup> showed that  $O_h$  isomers were favorable for Pt clusters. For perfect  $O_h$  isomers, their layers are all squares ( $n \times n$ ) and all eight surfaces are fcc (111) type. In general, the number of atoms for perfect  $O_h$  clusters is

$$N = 1^2 + \dots + n^2 + (n + 1)^2 + n^2 + \dots + 1^2. \quad (2)$$

On the other hand,  $I_h$  structures were also found to be favored for some metal clusters.<sup>56-59</sup> In addition, some quasicrystalline approximant crystals are based on icosahedral clusters.<sup>60</sup> For a perfect  $I_h$  structure, their 20 surfaces are all

fcc (111) type. The total number of atoms within the  $n$ th shell of perfect  $I_h$  structure is

$$N = [10(n+1)^3 + 15(n+1)^2 + 11(n+1) + 3]/3. \quad (3)$$

In the following, we will compare the binding energies of the stable  $I_h$  isomers with those of  $O_h$  structures in Fig. 2(b). In Fig. 2(b), the binding energies of  $I_h$  isomers (line with circles) and  $O_h$  fragments (line with triangles) are shown. Under the lines are the structures of  $O_h$  fragments. From Fig. 2(b), the binding energy of truncated  $O_h$   $Pb_{140}$  and  $Pb_{147}$  (seven atoms on one surface of  $O_h$   $Pb_{140}$ ) can compare with that of  $I_h$   $Pb_{146}$  (removing the center atom from  $I_h$   $Pb_{147}$ ) and  $Pb_{147}$ , while perfect  $O_h$   $Pb_{146}$  lies lower in the binding energy. Compared with  $O_h$  isomer  $Pb_{344}$ ,  $Pb_{338}$  (remove six vertexes from  $O_h$   $Pb_{344}$ ),  $Pb_{314}$  (remove six squares from  $O_h$   $Pb_{338}$ ),  $Pb_{309}$  (remove six  $1+2^2+3^2+4^2$  pyramids from  $O_h$   $Pb_{489}$ ), and  $Pb_{260}$  (remove six  $3 \times 3$  squares from  $O_h$   $Pb_{314}$ ),  $I_h$   $Pb_{309}$  lies lower in the binding energy, showing that the  $I_h$  structure is not favored at this size. From the slope of the curves, we conclude that  $I_h$   $Pb_{561}$  may be less stable than that of the  $O_h$  structure.

The differences of the average binding energy ( $E_b$ ), the highest occupied molecular orbital (HOMO)-lowest unoccupied molecular orbital (LUMO) gap ( $E_g$ ), the average bond length ( $R$ ), the nearest-neighbor atom number (NN), and the  $s$ - $p$  hybridization index ( $H_{sp}$ ) between the  $Pb_7$  unit-based isomers and the  $O_h$  fragments have been presented in Table I. In Table I, the average binding energy and the HOMO-LUMO gaps of the  $Pb_n$  isomers comprising  $Pb_7$  units lie higher than those of the  $O_h$  fragments up to  $n = 147$ , again explaining why  $Pb_7$  unit-based isomers are more stable. Although the  $Pb_7$  unit-based clusters have less average NN atoms than those of  $O_h$  fragments, the average bond length is usually smaller than that of  $O_h$  fragments up to  $n = 147$ . In addition, we compare the  $s$ - $p$  hybridization indices of  $Pb_n$  defined by

$$H_{sp} = \sum_{I=1}^n \sum_{i=1}^{\text{occ}} w_{i,s}^{(I)} w_{i,p}^{(I)}, \quad (4)$$

TABLE I. The differences of the average binding energies  $E_b$  (eV/atom), the HOMO-LUMO gap  $E_g$  (eV), the average bond length  $R$  (Å), the average nearest-neighbor atom numbers (NN), and the  $s$ - $p$  hybridization ( $H_{sp}$ ) index between the  $Pb_7$  unit-based isomers and the  $O_h$  fragments.

Size	$E_b$ (eV)	$E_g$ (eV)	$R$ (Å)	NN	$H_{sp}$
38	0.025	0.224	-0.022	-0.263	0.022
44	0.030	0.196	-0.001	-0.364	0.020
48	0.017	0.071	-0.020	-0.270	0.016
52	0.008	0.236	-0.005	-0.423	0.004
54	0.007	0.151	0.003	-0.259	0.007
62	0.008	0.009	-0.016	-0.387	0.000
66	0.007	0.105	-0.022	-0.394	0.009
70	0.005	0.057	-0.007	-0.486	0.010
79	0.006	0.214	-0.035	-0.937	0.026
146	0.014	0.113	-0.001	0.329	-0.003
147	0.018	0.077	-0.002	-0.170	0.011
309	-0.010	0.014	0.018	0.117	0.000

where  $w_{i,s}^{(I)}$  ( $w_{i,p}^{(I)}$ ) is the square of the projection of the  $i$ th Kohn-Sham orbital onto the  $s$  ( $p$ ) spherical harmonics centered at atom  $I$ , integrated over a sphere of radius equal to approximately half of the shortest NN distance in each cluster. The spin index is implicit in the sum of orbitals  $i$  in Eq. (4). In Table I,  $H_{sp}$  of  $Pb_7$  unit-based isomers are usually larger than those of  $O_h$  fragments, and thus the  $Pb_7$  unit-based isomers can be stabilized.<sup>61</sup> In other words,  $Pb_7$  unit-based clusters are energetically favored from  $Pb_7$  to  $I_h$   $Pb_{147}$ , and then the  $O_h$  isomers become more favorable gradually.

## IV. THE PROPERTIES OF $Pb_n$ CLUSTERS

### A. Radial distribution function

Because most  $Pb_n$  clusters are based on the building block of the  $Pb_7$  unit, it is natural to remind us that the properties of  $Pb_n$  clusters may have a relationship with the  $Pb_7$  cluster. To reveal this point, we give the radial distribution function (RDF) in Fig. 3, in which the red solid line at 3.56 Å is the distance between the nearest atoms in  $Pb$  bulk and the two dotted lines denote the borderlines 3 and 4 Å. The RDF shows the change of bond numbers with their corresponding bond lengths. By measuring the nearest atom distance, we find that less coordinated atoms (such as the vertexes of  $Pb_7$ ) always relate to a smaller bond length. Taking  $Pb_7$ , for example, the peak at 3.19 Å represents the 15 edge bonds, and the shorter

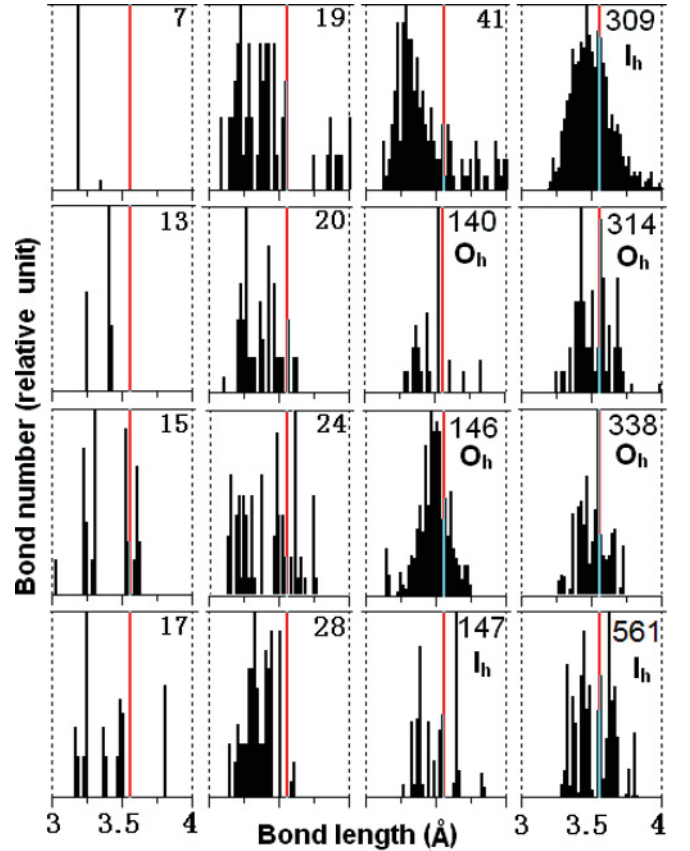


FIG. 3. (Color online) The changes of bond number (relative units) with bond-length distribution. The two dotted lines denote bond length 3 and 4 Å, while the red solid line 3.56 Å (the distance between the nearest atoms in  $Pb$  bulk), respectively.

line at 3.35 Å stands for the single bond in the pentagonal axis. For Pb<sub>13</sub>, the peak at 3.42 Å corresponds to the surface bonds. For Pb<sub>15</sub>, the peak at 3.30 Å is the bond number between the two regular hexagons, and the peak at 3.60 Å relates to the bond number connecting the two surface atoms at the hexagonal axis. For Pb<sub>17</sub>, the peak at 3.25 Å is the bond number between the atoms in two squares and the other surface atoms, the line at 3.18 Å is the eight bonds between the eight outermost atoms, and the line at 3.37 Å is the eight bonds in two squares. Compared with unstable Pb<sub>19</sub>, Pb<sub>20</sub> has a narrower bond-length distribution and a shorter average bond length. For Pb<sub>24</sub>, the bond length that is smaller than 3.20 Å is in the top hexagonal and the bottom triangle atoms, and the line at 3.37 Å is the bond number with the bottom distorted hexagon. For Pb<sub>28</sub> (C<sub>3v</sub>), the bond number distribution is relatively narrow and three inner atoms form an equilateral triangle, with a side length of 3.43 Å. The bond number distribution of Pb<sub>41</sub> has some peaks beyond 3.56 Å, showing its large structure. Compared with the truncated O<sub>h</sub> Pb<sub>140</sub> and I<sub>h</sub> isomer Pb<sub>147</sub>, the bond-length distribution of less stable isomers O<sub>h</sub> Pb<sub>146</sub> and I<sub>h</sub> Pb<sub>309</sub> becomes more spread, manifesting a larger structure relaxation. For truncated O<sub>h</sub> Pb<sub>314</sub> and Pb<sub>338</sub>, the bonds begin to accumulate at the bulk lattice constant 3.56 Å. The peaks of the I<sub>h</sub> isomer Pb<sub>147</sub> and Pb<sub>561</sub> accumulate at both sides of the bulk lattice constant, indicating different binding forms. In conclusion, the bond length in the Pb<sub>7</sub> unit is usually smaller than that between Pb<sub>7</sub> units, the peak of bond length density approaches a bulk value as the cluster size increases, and a distinct bond number distribution usually corresponds to more symmetric and more stable structures.

**B. Electronic oscillation and energy gap**

To exhibit the relative stabilities of Pb<sub>n</sub> (n = 6–33) clusters, we display the second-order difference of energies,

$$\Delta^2 E = E_{n+1} + E_{n-1} - 2E_n, \quad (5)$$

in Fig. 4(a), from which Pb<sub>n</sub> (n = 7, 10, 13, 15, 17, 20, 24, and 28) exhibits peaks in the Δ<sup>2</sup>E curve, indicating a higher stability than their neighbors. With more neighbor atoms, the inner atoms are usually the vertexes of the Pb<sub>7</sub> units, which cause us to study the electronic properties as the inner atoms increase. As shown in Fig. 4(b), the inner atom number in the Pb<sub>n</sub> (n = 6–33) clusters increases steadily, and such changes in geometrical structures can also be reflected from the s and p electron oscillation by projecting the valence charge in the Wigner-Seitz sphere (1.81 Å) onto an atomic orbital, as shown in Figs. 4(c) and 4(d), respectively, in which hollow (solid) circles are the average electrons per atom (inner atom). Although the space division is somewhat arbitrary, the obtained results are almost Wigner-Seitz-sphere independent and can qualitatively provide important information about the electronic structures of Pb clusters. In Figs. 4(c) and 4(d), the inner atoms usually have more electrons and stronger oscillation, explaining why they are usually one of the vertexes of Pb<sub>7</sub> units and have more neighbor atoms. In addition, the electronic oscillation is mainly contributed by p electrons, showing p electrons are extranuclear electrons. From the smallest to the largest N atom-centered clusters, p electrons per inner atom decrease rapidly, while one inner atom of Pb<sub>30</sub>

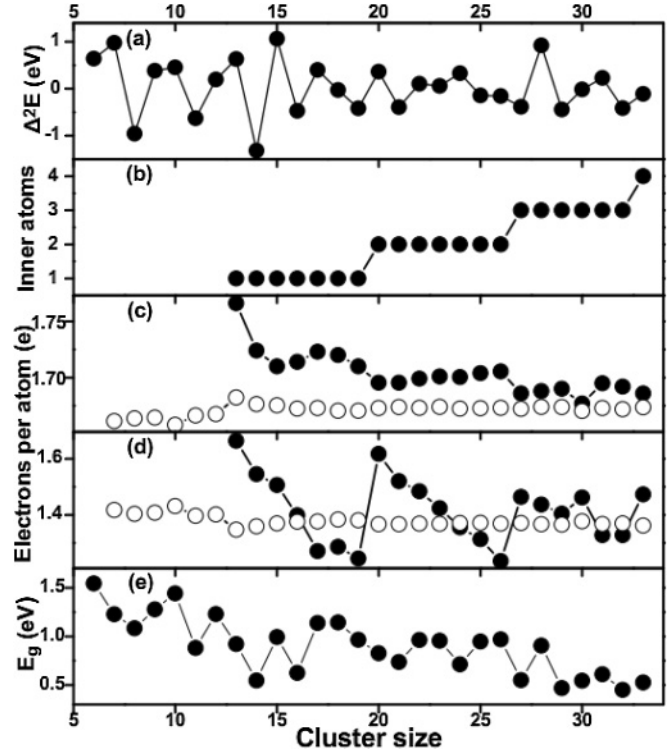


FIG. 4. (a) Second-order difference of energies, Δ<sup>2</sup>E = E<sub>n+1</sub> + E<sub>n-1</sub> - 2E<sub>n</sub>. (b) Inner atom number with respect to the cluster size. (c) Open (solid) circles are the s electrons per atom (inner atom). (d) Open (solid) circles are the p electrons per atom (inner atom). (e) Energy gap (eV), which is the energy difference between the lowest unoccupied and the highest occupied energy levels.

is not the vertex of the Pb<sub>7</sub> unit, making it an exception. Figure 4(e) shows that HOMO-LUMO gaps decrease (with some oscillations) as cluster size increases. In most cases, more stable clusters have larger HOMO-LUMO gaps. Also, the HOMO-LUMO gaps at the smallest (largest) N atom-centered clusters always show smaller (larger) values, indicating they are more (less) compact.

**C. Electronic density of states**

The electronic density of states (DOS) is usually considered as a tool connecting the experimental and theoretical results. In Fig. 5, the total electronic DOS for the ground states of Pb<sub>n</sub> clusters and bulk Pb have been shown by expanding the eigenvalues in Lorentz form, in which the Fermi level has been shifted to zero. The discrete spectra of small Pb<sub>n</sub> (n = 13, 15, 17, 24 and 28) clusters resemble those of Pb<sub>7</sub>. Beginning from Pb<sub>41</sub>, the spectrum becomes more continuous, showing some metallic characters. The spectra of I<sub>h</sub> Pb<sub>147</sub> isomers still show strong discrete peaks, indicating some common features with small Pb<sub>7</sub> unit-based clusters. Larger O<sub>h</sub> isomers Pb<sub>338</sub>, Pb<sub>489</sub>, and Pb<sub>561</sub> begin to manifest bulk spectrum features, however, by the Fermi level, the difference from the bulk spectrum is significant, as almost all the faces of O<sub>h</sub>(I<sub>h</sub>) clusters are fcc (111) type, and atoms at the edges and vertexes have less neighbor atoms.<sup>2</sup>

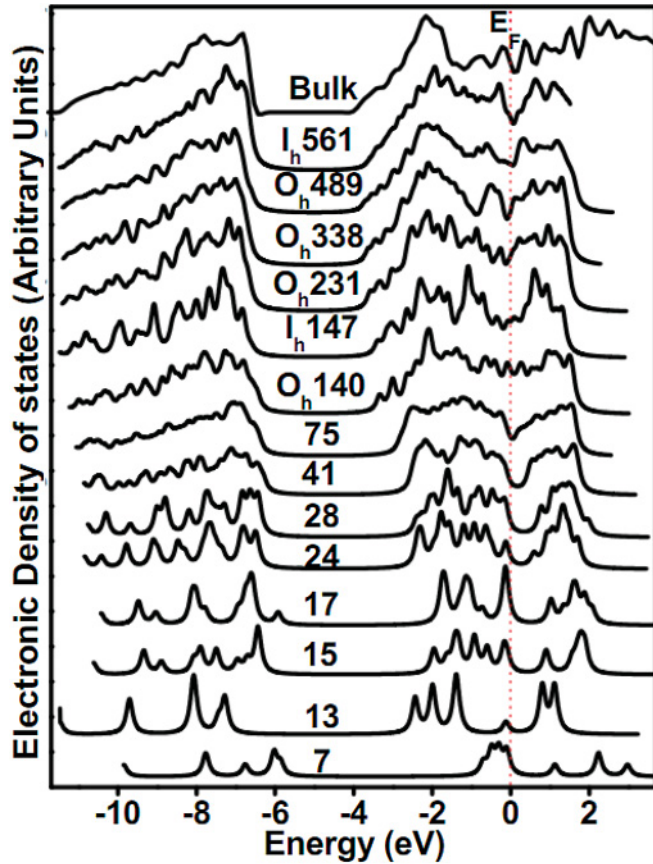


FIG. 5. (Color online) Electronic DOS (arbitrary units) for  $Pb_n$  clusters by expanding the eigenvalues in Lorentz form. The Fermi energies ( $E_F$ ) have been shifted to zero.

## V. COVALENT BINDING CHARACTER

### A. Charge density of a covalently bonded $Pb_7$ unit in $Pb_n$ clusters

To elaborate on the relationship between the geometrical structures and the binding characters of  $Pb_n$  clusters, we show the atom distribution and the electronic charge difference,

$$\Delta\rho = \rho(SC) - \rho(SP), \quad (6)$$

of  $Pb_7$  in Figs. 6(a) and 6(b). Here,  $\Delta\rho$  is the averaged charge-density difference along the axis of the bonds shown in a normalized scale,  $\rho(SC)$  is obtained by a self-consistent calculation, and  $\rho(SP)$  is the superposition of the atomic charge for the same structure. As presented in Fig. 6(b), electrons accumulate considerably at the center of atoms 1 and 2 (in purple circles), revealing a strong covalent binding character between the nearest pentagonal atoms. Electrons accumulate less densely at the center of atoms 1 and 3 (in blue squares) but deplete between atoms 3 and 4 (in orange pentagons). Figure 6(c) gives the charge difference of the plane containing number 1, 3, and 4 atoms, in which significant electron accumulation between atoms 6 and 7 is shown in red at the right-hand side and electrons depleting between atoms 3 and 4 are shown in blue zones. Figure 6(d) gives the charge difference of the plane containing number 1, 2, and 5 atoms, in which obvious electron accumulation is

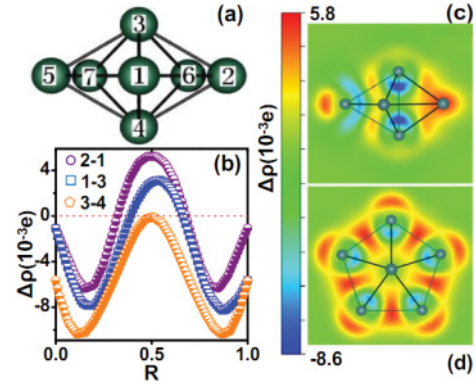


FIG. 6. (Color online) (a) The atom distribution of  $Pb_7$ . (b) Averaged charge-density differences,  $\Delta\rho$ , along the axis of the bonds of two atoms, with the bond lengths shown in normalized scale. (c) Averaged charge-density differences of the plane containing number 1, 3, and 4 atoms. (d) Averaged charge-density differences of the plane containing number 1, 2, and 5 atoms.

shown between the nearest pentagonal atoms. In fact, Kirihara *et al.*<sup>60</sup> found a covalent binding character in  $\alpha$ -Al(Mn,Re)Si (quasicrystalline approximant alloy crystals) and attributed it to the enhancement of the electron DOS pseudogap near the Fermi level. Recently, we have also found strong covalent bonds in  $Ru_n$  ( $n = 14-42$ ) clusters and associated them with strong  $s$ - $d$  hybridization.<sup>62</sup>

Owing to the unequal neighbor atoms,  $Pb_7$  units in larger clusters will undergo distortion. The atom distribution and the electronic charge difference of  $Pb_{28}$  (the same structure as in Fig. 1, from another viewing angle) are shown in Figs. 7(a) and 7(b), in which  $\Delta\rho$  in the  $Pb_7$  unit is smaller than that in the isolated  $Pb_7$  cluster, showing that the covalent binding character weakens as cluster size increases. In addition, the bond between surface atoms in different  $Pb_7$  units (atoms 6 and 7) also shows a covalent character, which may stabilize  $Pb_n$  clusters and increase their melting point.

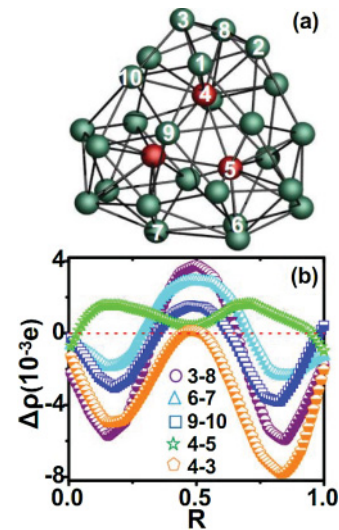


FIG. 7. (Color online) (a) The atom distribution of  $Pb_{28}$ . (b) Averaged charge-density differences,  $\Delta\rho$ , along the axis of the bonds of two atoms, with the bond lengths shown in normalized scale.

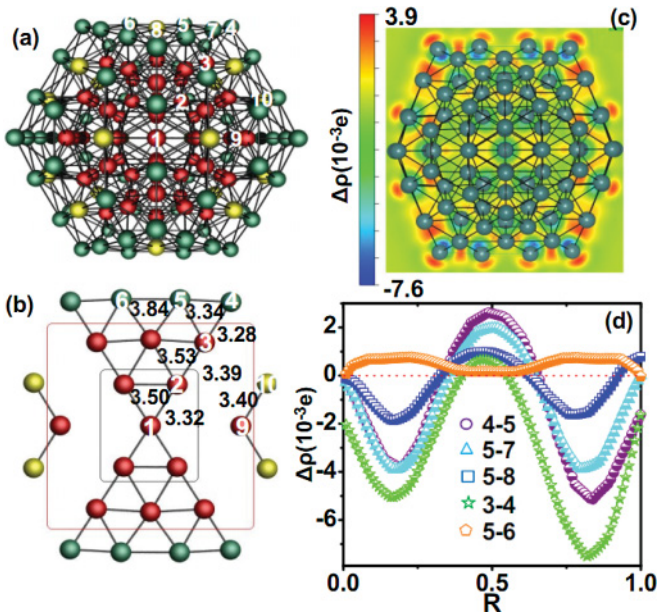


FIG. 8. (Color online) (a) Structure of  $I_h$  Pb<sub>147</sub>: The green (yellow) atoms stand for the surface atoms belonging (not belonging) to Pb<sub>7</sub> units and the red atoms are the inner atoms. (b) The atom distribution of the middle section of  $I_h$  Pb<sub>147</sub>. (c) Averaged charge-density differences of the middle section. (d) Averaged charge-density differences,  $\Delta\rho$ , along the axis of the bonds between different atoms.

As mentioned above, the bond length in covalently bonded Pb<sub>7</sub> units is usually shorter. Pb<sub>7</sub> units not only stabilize Pb clusters but also obstruct the electronic delocalization process. Besides the basic building block Pb<sub>7</sub> units, there should be some “glue” atoms to combine Pb<sub>7</sub> units. For Pb<sub>7</sub>-based Pb<sub>19</sub> ( $C_{5v}$ ), three independent Pb<sub>7</sub> units are connected weakly by two common inner atoms, making it (0.06 eV/atom) less favorable than that of the ground state (in Fig. 1). If the core of  $I_h$  Pb<sub>55</sub> retains the same proportion as  $I_h$  Pb<sub>13</sub> and all the surface atoms belong to Pb<sub>7</sub> units, the distance between the nearest surface atoms may be more than 3.5 Å. But owing to the covalent binding character of Pb<sub>7</sub> units, some surface atoms cluster to form four Pb<sub>7</sub> units and cause  $I_h$  Pb<sub>55</sub> to break.

The atom distribution and the electronic charge difference of Pb<sub>147</sub> are shown in Figs. 8(a) and 8(b). Figure 8(a) shows that 72 surface atoms (in green) of  $I_h$  Pb<sub>147</sub> belong to 12 independent Pb<sub>7</sub> units, leaving 20 surface atoms (in yellow) on the center of 20 surfaces. Figure 8(b) gives the atom distribution of one middle section, in which the atoms in black and red rectangles belong to the inner  $I_h$  Pb<sub>13</sub> and Pb<sub>55</sub> atoms, respectively. The surface bond lengths of the inner 13 and 55 atoms are 3.50 and 3.53 Å, respectively, while they are 3.34 Å for the surface atoms in Pb<sub>7</sub> unit and 3.84 Å between Pb<sub>7</sub> units. The geometrical properties can also be reflected from electronic structures in Fig. 8(c) [Fig. 8(d)], which show obvious electron accumulation in covalently bonded Pb<sub>7</sub> units.  $I_h$  Pb<sub>309</sub> is not that symmetric: Its 72 surface atoms belong to 12 Pb<sub>7</sub> units and 90 surface atoms scatter loosely on the center of 20 surfaces, making it less stable than  $O_h$  isomers. Similar to  $I_h$  Pb<sub>147</sub>,  $I_h$  Pb<sub>561</sub> shows significant Pb<sub>7</sub> units, whose 72 surface atoms belong to 12 Pb<sub>7</sub> units and 180 surface atoms

can form some quaternary clusters on the center of 20 surfaces. To the best of our knowledge, such covalent characters were never reported for other metal clusters up to that large size. We also test  $I_h$  isomers of Al<sub>147</sub> and find its atoms (charge density) distribute evenly on each surface, showing metallic characters. In addition, we also find such a covalent binding character in the  $I_h$  Sn<sub>147</sub> cluster.

**B. Relationship between covalent bond and thermal stabilities**

To study the relationship between the covalent binding character and thermal stabilities, we carried out the *ab initio* MD simulations on some low-lying isomers. Figure 9(a) shows the changes of bond length (BL) (Å) in Pb<sub>28</sub> with the MD steps (1 fs/step). The red squares (black triangles) stand for the BL between atoms 6 and 7 (atoms 1 and 2) at constant temperature 700 K. Figure 9(b) is the same as Fig. 9(a), with  $T = 750$  K. The structures in Figs. 9(a) and 9(b) are the initial state for both temperatures and the optimized final state after 2500 MD steps at 750 K, respectively. At 700 K, the BL of atoms 6 and 7 can fall back to the initial value and, selecting the structures at random steps for Pb<sub>28</sub> [the same structure as in Fig. 7(a)] as the initial configuration to relax, we can always obtain the initial structure. For MD simulation at 750 K, the BL of atoms 6 and 7 can be larger than 6 Å, and selecting the structure at 2500 steps to relax, we get the final structure in Fig. 9(b), which is 0.66 eV less stable than the initial structure, while choosing the structure at 5000 steps to relax, we get the initial structure again. The oscillation of BL between atoms 1 and 2 is weaker, showing the covalent bond in the Pb<sub>7</sub> unit is stronger than that between the Pb<sub>7</sub> units.

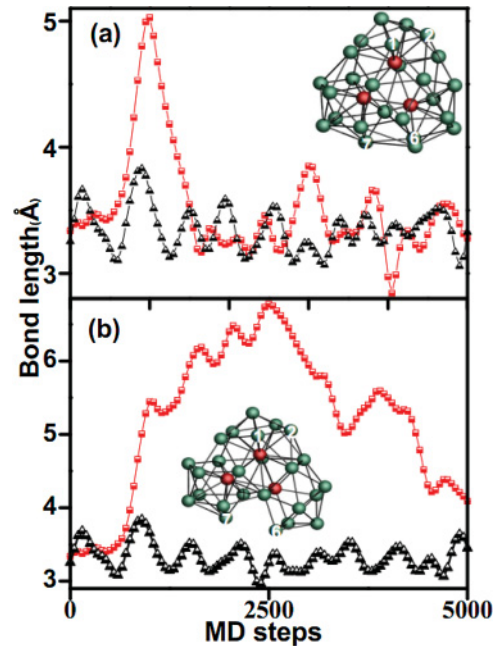


FIG. 9. (Color online) (a) The changes of bond length (Å) in Pb<sub>28</sub> vary with the MD steps (1 fs/step). The red squares (black triangles) stand for the BL between atoms 6 and 7 (atoms 1 and 2) at constant temperature 700 K. (b) The same as (a), with  $T = 750$  K. The structure in (a) is the initial state and (b) is the optimized final state after 2500 MD steps at 750 K.

The above descriptions may demonstrate that  $Pb_{28}$  favors its ground state when the temperature is 100–150 K higher than its bulk melting point (588 K for DFT calculations of Lindemann melting temperature<sup>40</sup> and 600 K for experiment). With the same standard in our calculations, the  $Pb_n$  ( $n = 12, 13, 15, 16, 18, 20, 21, 23,$  and  $25$ ) cluster favors its ground state when the temperature is higher than 750 K, the  $Pb_n$  ( $n = 14, 17, 22, 30$ ) cluster prefers its ground state between 700 and 750 K, and the  $Pb_n$  ( $n = 26, 27, 29$ ) favors its ground state between 650 and 700 K.  $Pb_{24}$  prefers its ground state between 600 and 650 K, while  $Pb_{19}$  is unstable when the temperature is higher than 600 K. Choosing the structures at a random step of constant MD simulation 650 K for  $Pb_{36}$  (with  $Pb_7$  units), we can always obtain the initial structure. These findings may support the bond stiffening<sup>40</sup> theoretical prediction that  $Pb_n$  nanoclusters possess a higher melting point than that of their bulk counterparts, and the existence of significant covalent bonding in metal clusters may also hold for explaining why some Sn and Pb clusters remain solid above the bulk melting temperature.<sup>42–44</sup>

## VI. SUMMARY

In summary, we have systematically studied the geometric and electronic characters of  $Pb_n$  clusters from dimer to nanoparticles with diameters up to 3 nm. As distinguished

from prolate Si, Ge, and Sn clusters, amorphouslike  $Pb_n$  clusters with more independent  $Pb_7$  units are magic and relatively stable, which are more favorable than  $O_h$  fragments up to  $n = 147$ . Although the  $Pb_7$  unit-based clusters have less average NN atoms than those of  $O_h$  fragments, the average bond length ( $E_g$  and  $H_{sp}$ ) is usually smaller (larger) than that of the  $O_h$  fragments. Owing to the covalent binding characters of the  $Pb_7$  unit, the charge density in the  $Pb_7$  unit is usually higher than that between  $Pb_7$  units. Covalently bonded  $Pb_7$  units not only stabilize the Pb cluster, but also obstruct the electronic delocalization. The spectrum character of  $I_h$   $Pb_{147}$  isomers still shows strong discrete peaks, indicating some common features with small  $Pb_7$  unit-based clusters, while larger isomers begin to manifest bulk spectrum features. Owing to the bond stiffness of the  $Pb_7$  unit,  $Pb_n$  ( $n < 31$ ) clusters are usually favored when the temperature is higher than the melting point of bulk. By tracing two bond lengths in the  $Pb_7$  unit and between the  $Pb_7$  units, we find that the melting process begins from the bond between  $Pb_7$  units, which again manifests the existence of covalent bonding in  $Pb_n$  clusters.

## ACKNOWLEDGMENTS

This work was supported by the NSF of China (Grant No. 10974182) and the Outstanding Young Foundations in Henan Province.

\*jiayu@zzu.edu.cn

- <sup>1</sup>M. Schmidt, R. Kusche, W. Kronmüller, B. von Issendorff, and H. Haberland, *Phys. Rev. Lett.* **79**, 99 (1997).
- <sup>2</sup>V. Kumar and Y. Kawazoe, *Phys. Rev. B* **77**, 205418 (2008).
- <sup>3</sup>P. J. Roach, W. H. Woodward, A. W. Castleman Jr., A. C. Reber, and S. N. Khanna, *Science* **295**, 99 (2002).
- <sup>4</sup>M. F. Jarrold and V. A. Constant, *Phys. Rev. Lett.* **67**, 2994 (1991).
- <sup>5</sup>V. E. Bazterra, O. Oña, M. C. Caputo, M. B. Ferraro, P. Fuentealba, and J. C. Facelli, *Phys. Rev. A* **69**, 053202 (2004).
- <sup>6</sup>W. Hellmann, R. G. Hennig, S. Goedecker, C. J. Umrigar, B. Delley, and T. Lenosky, *Phys. Rev. B* **75**, 085411 (2007).
- <sup>7</sup>P. L. Tereshchuk, Z. M. Khakimov, F. T. Umarova, and M. T. Swihart, *Phys. Rev. B* **76**, 125418 (2007).
- <sup>8</sup>R. L. Zhou and B. C. Pan, *J. Chem. Phys.* **128**, 234302 (2008).
- <sup>9</sup>R. L. Zhou, L. Y. Zhao, and B. C. Pan, *J. Chem. Phys.* **131**, 034108 (2009).
- <sup>10</sup>S. J. Peppernick, K. D. D. Gunaratne, S. G. Sayres, and A. W. Castleman Jr., *J. Chem. Phys.* **132**, 044302 (2010).
- <sup>11</sup>J. M. Hunter, J. L. Fye, M. F. Jarrold, and J. E. Bower, *Phys. Rev. Lett.* **73**, 2063 (1994).
- <sup>12</sup>J. L. Wang, G. H. Wang, and J. J. Zhao, *Phys. Rev. B* **64**, 205411 (2001).
- <sup>13</sup>S. Yoo and X. C. Zeng, *J. Chem. Phys.* **124**, 184309 (2006).
- <sup>14</sup>W. Qin, W. C. Lu, Q. J. Zang, L. Z. Zhao, G. J. Chen, C. Z. Wang, and K. M. Ho, *J. Chem. Phys.* **131**, 124507 (2009).
- <sup>15</sup>W. Qin, W. C. Lu, Q. J. Zang, L. Z. Zhao, G. J. Chen, C. Z. Wang, and K. M. Ho, *J. Chem. Phys.* **132**, 214509 (2010).
- <sup>16</sup>A. A. Shvartsburg and M. F. Jarrold, *Phys. Rev. A* **60**, 1235 (1999).
- <sup>17</sup>T. Bachelis, R. Schäfer, and H.-J. Güntherodt, *Phys. Rev. Lett.* **84**, 4890 (2000).

- <sup>18</sup>C. Majumder, V. Kumar, H. Mizuseki, and Y. Kawazoe, *Phys. Rev. B* **64**, 233405 (2001).
- <sup>19</sup>C. Majumder, V. Kumar, H. Mizuseki, and Y. Kawazoe, *Phys. Rev. B* **71**, 035401 (2005).
- <sup>20</sup>L. F. Cui, L. M. Wang, and L. S. Wang, *J. Chem. Phys.* **126**, 064505 (2007).
- <sup>21</sup>E. Oger, R. Kelting, P. Weis, A. Lechtken, D. Schooss, N. R. M. Crawford, R. Ahlrichs, and M. M. Kappes, *J. Chem. Phys.* **130**, 124305 (2009).
- <sup>22</sup>A. Lechtken, N. Drebov, R. Ahlrichs, M. M. Kappes, and D. Schooss, *J. Chem. Phys.* **132**, 211102 (2010).
- <sup>23</sup>A. A. Shvartsburg and M. F. Jarrold, *Chem. Phys. Lett.* **317**, 615 (2000).
- <sup>24</sup>M. M. Özer, Y. Jia, B. Wu, Z. Y. Zhang, and H. H. Weitering, *Phys. Rev. B* **72**, 113409 (2005).
- <sup>25</sup>P. Czoschke, H. Hong, L. Basile, and T.-C. Chiang, *Phys. Rev. B* **72**, 075402 (2005).
- <sup>26</sup>Y. Jia, B. Wu, H. H. Weitering, and Z. Y. Zhang, *Phys. Rev. B* **74**, 035433 (2006).
- <sup>27</sup>J. H. Dil, F. Meier, J. Lobo-Checa, L. Patthey, G. Bihlmayer, and J. Osterwalder, *Phys. Rev. Lett.* **101**, 266802 (2008).
- <sup>28</sup>Y. Saito, K. Yamauchi, K. Mihama, and T. Noda, *Jpn. J. Appl. Phys.* **21**, L396 (1982).
- <sup>29</sup>K. L. Hing, R. G. Wheeler, W. L. Wilson, and M. A. Duncan, *J. Chem. Phys.* **87**, 3401 (1987).
- <sup>30</sup>K. Sattler, J. Mühlbach, O. Echt, P. Pfau, and E. Recknagel, *Phys. Rev. Lett.* **47**, 160 (1981).
- <sup>31</sup>L. F. Cui, X. Huang, L. M. Wang, J. Li, and L. S. Wang, *J. Phys. Chem. A* **110**, 10169 (2006).
- <sup>32</sup>C. H. Lüder and K. H. Meiwes-Broer, *Chem. Phys. Lett.* **294**, 391 (1998).

- <sup>33</sup>S. Peredkov, S. L. Sorensen, A. Rosso, G. Öhrwall, M. Lundwall, T. Rander, A. Lindblad, H. Bergersen, W. Pokapanich, S. Svensson, O. Björneholm, N. Mårtensson, and M. Tchapyguine, *Phys. Rev. B* **76**, 081402(R) (2007).
- <sup>34</sup>V. Senz, T. Fischer, P. Oelßner, J. Tiggesbäumker, J. Stanzel, C. Bostedt, H. Thomas, M. Schöffler, L. Foucar, M. Martins, J. Neville, M. Neeb, Th. Möller, W. Wurth, E. Rühl, R. Dörner, H. Schmidt-Böcking, W. Eberhardt, G. Ganteför, R. Treusch, P. Radcliffe, and K.-H. Meiwes-Broer, *Phys. Rev. Lett.* **102**, 138303 (2009).
- <sup>35</sup>B. L. Wang, J. J. Zhao, X. S. Chen, D. N. Shi, and G. H. Wang, *Phys. Rev. A* **71**, 033201 (2005).
- <sup>36</sup>C. Rajesh, C. Majumder, M. G. R. Rajan, and S. K. Kulshreshtha, *Phys. Rev. B* **72**, 235411 (2005).
- <sup>37</sup>C. Rajesh and C. Majumder, *J. Chem. Phys.* **126**, 244704 (2007).
- <sup>38</sup>Xiao-Ping Li, Wen-Cai Lu, Qing-Jun Zang, Guang-Ju Chen, C. Z. Wang, and K. M. Ho, *J. Phys. Chem. A* **113**, 6217 (2009).
- <sup>39</sup>S. C. Hendy and J. P. K. Doye, *Phys. Rev. B* **66**, 235402 (2002).
- <sup>40</sup>R. Pushpa, U. Waghmare, and S. Narasimhan, *Phys. Rev. B* **77**, 045427 (2008).
- <sup>41</sup>W. H. Luo, W. Y. Hu, and S. F. Xiao, *J. Chem. Phys.* **128**, 074710 (2008).
- <sup>42</sup>A. A. Shvartsburg and M. F. Jarrold, *Phys. Rev. Lett.* **85**, 2530 (2000).
- <sup>43</sup>K. Joshi, D. G. Kanhere, and S. A. Blundell, *Phys. Rev. B* **67**, 235413 (2003).
- <sup>44</sup>F. C. Chuang, C. Z. Wang, S. Ögüt, J. R. Chelikowsky, and K. M. Ho, *Phys. Rev. B* **69**, 165408 (2004).
- <sup>45</sup>J. P. Perdew and Y. Wang, *Phys. Rev. B* **45**, 13244 (1992).
- <sup>46</sup>G. Kresse and J. Furthmüller, *Phys. Rev. B* **54**, 11169 (1996).
- <sup>47</sup>G. Kresse and J. Furthmüller, *Comput. Mater. Sci.* **6**, 15 (1996).
- <sup>48</sup>P. E. Blöchl, *Phys. Rev. B* **50**, 17953 (1994).
- <sup>49</sup>G. Kresse and D. Joubert, *Phys. Rev. B* **59**, 1758 (1999).
- <sup>50</sup>M. P. Teter, M. C. Payne, and D. C. Allan, *Phys. Rev. B* **40**, 12255 (1989).
- <sup>51</sup>Y. Wang, S. Curtarolo, C. Jiang, R. Arroyave, T. Wang, G. Ceder, L.-Q. Chen, and Z.-K. Liu, *CALPHAD: Computer Coupling of Phase Diagrams and Thermochemistry* **28**, 79 (2004).
- <sup>52</sup>S. F. Li, H. S. Li, J. Liu, X. L. Xue, Y. T. Tian, H. He, and Y. Jia, *Phys. Rev. B* **76**, 045410 (2007).
- <sup>53</sup>Xiao-Ping Li, Wen-Cai Lu, C. Z. Wang, and K. M. Ho, *J. Phys. Condens. Matter* **22**, 465501 (2010).
- <sup>54</sup>K. Thürmer, J. E. Reutt-Robey, E. D. Williams, M. Uwaha, A. Emundts, and H. P. Bonzel, *Phys. Rev. Lett.* **87**, 186102 (2001).
- <sup>55</sup>C. Brun, I-Po Hong, F. Patthey, I. Y. Sklyadneva, R. Heid, P. M. Echenique, K. P. Bohnen, E. V. Chulkov, and W. D. Schneider, *Phys. Rev. Lett.* **102**, 207002 (2009).
- <sup>56</sup>D. Y. Sun and X. G. Gong, *Phys. Rev. B* **57**, 4730 (1998).
- <sup>57</sup>V. Kumar and Y. Kawazoe, *Phys. Rev. B* **63**, 075410 (2001).
- <sup>58</sup>V. G. Grigoryan, D. Alamanova, and M. Springborg, *Phys. Rev. B* **73**, 115415 (2006).
- <sup>59</sup>R. Singh and P. Kroll, *Phys. Rev. B* **78**, 245404 (2008).
- <sup>60</sup>K. Kirihara, T. Nagata, K. Kimura, K. Kato, M. Takata, E. Nishibori, and M. Sakata, *Phys. Rev. B* **68**, 014205 (2003).
- <sup>61</sup>C. M. Chang and M. Y. Chou, *Phys. Rev. Lett.* **93**, 133401 (2004).
- <sup>62</sup>S. F. Li, H. S. Li, X. L. Xue, Y. Jia, Z. X. Guo, Z. Y. Zhang, and X. G. Gong, *Phys. Rev. B* **82**, 035443 (2010).